Low-energy near Earth asteroid capture using Earth flybys and aerobraking

Minghu Tan*

School of Engineering, University of Glasgow, Glasgow G12 8QQ, UK

Colin McInnes and Matteo Ceriotti

School of Engineering, University of Glasgow, Glasgow G12 8QQ, UK

Abstract

Since the Sun-Earth libration points L_1 and L_2 are regarded as ideal locations for space science missions and candidate gateways for future crewed interplanetary missions, capturing near-Earth asteroids (NEAs) around the Sun-Earth L_1/L_2 points has generated significant interest. Therefore, this paper proposes the concept of coupling together a flyby of the Earth and then capturing small NEAs onto Sun–Earth L_1/L_2 periodic orbits. In this capture strategy, the Sun-Earth circular restricted three-body problem (CRTBP) is used to calculate target Lypaunov orbits and their invariant manifolds. A periapsis map is then employed to determine the required perigee of the Earth flyby. Moreover, depending on the perigee distance of the flyby, Earth flybys with and without aerobraking are investigated to design a transfer trajectory capturing a small NEA from its initial orbit to the stable manifolds associated with Sun-Earth L_1/L_2 periodic orbits. Finally, a global optimization is carried out, based on a detailed design procedure for NEA capture using an Earth flyby. Results show that the NEA capture strategies using an Earth flyby with and without aerobraking both have the potential to be of lower cost in terms of energy requirements than a direct NEA capture strategy without the Earth flyby. Moreover, NEA capture with an Earth flyby also has the potential for a shorter flight time compared to the NEA capture strategy without the Earth flyby.

Keywords: Circular restricted three-body problem; Lyapunov orbit; stable manifolds; Earth flyby; aerobraking

* Corresponding author.

E-mail address: m.tan.2@research.gla.ac.uk (Minghu Tan).

1. Introduction

Near-Earth Asteroids (NEAs) can in principle provide useful resources in terms of feedstock for spacecraft propellant, crew logistic support and a range of useful metals (Sonter, 1997). The exploitation of these in-situ resources has long been proposed as a necessary part of long-term space development (Lewis and Hutson, 1993; Bottke, 2002; Sanchez et al., 2012; Yárnoz et al., 2013). Therefore, the idea of capturing NEAs, based on current technology, for scientific and potentially commercial purposes, has been studied in recent work (Hasnain et al., 2012; Sanchez et al., 2012; Lladó et al., 2014; Sánchez and Yárnoz, 2016). In these works, the Sun-Earth collinear libration points L_1 and L_2 repeatedly appear as ideal locations for captured NEAs (Yárnoz et al., 2013; Lladó et al., 2014; Sánchez and Yárnoz, 2016).

The Sun-Earth L_1 and L_2 points are so noteworthy due to their unique locations and dynamical characteristics. The Sun–Earth L_1 point is an ideal position for scientific observations of the Sun–Earth system, such as monitoring the solar wind. Similarly, the Sun–Earth L_2 point is also a useful location for space-based observatories and is regarded as a staging node for interplanetary missions to NEAs and Mars (Farquhar et al., 2004). Overall, the Sun-Earth L_1 and L_2 points represent potentially beneficial gateways for future interplanetary missions (Zimmer, 2013). Periodic orbits around these collinear libration points have an unstable behaviour and will consequently diverge under a small perturbation. The trajectories generated from a periodic orbit under such perturbations are the invariant manifolds associated with the periodic orbit. Hence, such periodic orbits and their associated invariant manifolds can be employed to investigate low-cost transfer trajectories between different orbits (Lo and Parker, 2004; Davis et al., 2011; Xu et al., 2012). After a spacecraft moves onto the stable manifold of a libration point orbit (LPO), it will transfer to the target periodic orbit without any further manoeuvres. Meanwhile, such dynamical characteristics have been widely used in various trajectory design problems, including transfers between LPOs within the circular restricted three-body problem (CRTBP) of the Sun-Earth system (Davis et al., 2010; 2011; Xu et al., 2012). Furthermore, invariant manifolds are also proposed as a basic design strategy to calculate connections between different dynamical systems, such as low energy transfers between the Earth–Moon CRTBP and Sun–Earth CRTBP (Koon et al., 2000; Koon et al., 2001; Howell and Kakoi, 2006; Koon et al., 2011; Lei and Xu, 2016) . In these studies, transfers between two different three-body systems can be modelled by patching together invariant manifold tubes from each system. Usually a manoeuvre at or near the patching point is needed to move the spacecraft from one manifold tube to the other.

Following the interest in capturing NEAs onto Sun-Earth LPOs, continuous-thrust propulsion has been considered to capture NEAs to LPOs around the Sun–Earth L_2 point (Lladó et al., 2014). Meanwhile, a family of Easily Retrievable Objects (EROs) has been defined, corresponding to a subset of NEAs which are captured onto the Sun–Earth L_1 or L_2 periodic orbits with a total cost below 500 m/s (Yárnoz et al., 2013). Accordingly, the list of EROs have been updated (Sánchez and Yárnoz, 2016) and low thrust has been considered to design retrieval trajectories (Mingotti et al., 2014; Tang and Jiang, 2016). Meanwhile, work on low-energy transfers between Sun-Earth LPOs and NEAs has also been undertaken. The Sun–Earth L_2 point is regarded as an important gateway for NEA and Mars exploration missions (Farquhar et al., 2004). For low-energy crewed exploration of NEAs, Zimmer (2013) proposed to employ a reusable spacecraft that is stationed on a halo orbit at the Sun-Earth L_1 or L_2 point for such missions. A perturbation method has been proposed to search for possible flyby opportunities between Sun-Earth Lissajous orbits and the asteroids Toutatis and 2010 JK1. The method then calculates low-energy transfers between the Lissajous orbit and the asteroids (Wang et al., 2013). Then Gao (2013) investigated optimal bi-impulse flyby trajectories from the Sun-Earth L_2 point to the asteroids Toutatis, 2005 NZ6 and 2010 CL19. Besides, the Earth-Moon collinear libration points L_1 and L_2 are also viewed as potential staging points for future NEA exploration. NASA has also proposed a near-Earth asteroid redirect mission (ARM) to capture and return an NEA (or part of an NEA) to the Earth–Moon system and place it into a distant retrograde orbit around the Moon (Brophy et al., 2012).

Gravity assists have also played a significant role in interplanetary mission design and deep space exploration. The concept of the gravity assist was proposed by Minovitch after he developed the patched conic method and accordingly it was used to design a range of low-cost interplanetary trajectories (Minovitch, 2010). Gravity assists can provide extended opportunities for interplanetary exploration, including NEA missions. Earth Gravity Assists (EGAs) were investigated to reduce the launch energy and the total cost of two-impulse transfer trajectories to NEAs (Qiao et al., 2006). EGA is also utilized to reduce the total cost of transporting a small asteroid to impact a larger hazardous asteroid (Eismont et al., 2013). Moreover, Mars gravity assists and solar electric propulsion were applied to design low-cost transfer trajectories to the main belt asteroids (Casalino and Colasurdo, 2003) and it has been shown that Mars is the most useful gravity-assist body for main-belt asteroid exploration through the utilization of Tisserand graphs (Chen et al., 2014). Multiple gravity assists (MGAs) based on a hybrid approach were applied to design interplanetary transfers both to the asteroids and comets (Vasile and Pascale, 2006). MGAs can be also used to design transfer trajectories between an NEA and a main-belt asteroid (Yang et al., 2015). As for asteroid capture missions, a lunar flyby was used to capture an

NEA temporarily into the Earth's Hill region (Gong and Li, 2015). Gravity assists were also investigated to capture NEAs into bound orbits around the Earth (Bao et al., 2015).

Low energy trajectory design in multi-body environments is a rich and active research area which focuses on various classes of orbit design problems. As noted earlier, the utilization of periodic orbits and their associated invariant manifolds, to design low-energy trajectories in multi-body systems, has been a topic of particular interest in recent years (Folta et al., 2012; Pavlak, 2013). Weak Stability Boundary (WSB) theory has also been proposed and developed to design low energy Earth-Moon transfers (Belbruno and Miller, 1993). To design transfer trajectories in multi-body environments, efficient mathematical tools are necessary, including the shooting method and Poincaré maps. Since the multiple shooting method can significantly reduce the dynamical sensitivities of the trajectories associated with LPOs, it has been studied extensively to obtain solutions of the boundary value problems (BVP) in the CRTBP (Keller, 1976; Grebow, 2010). Moreover, the Poincaré map that employs common hyper-plane definitions in a rotating reference frame can be used to transform a continuous time system to a discrete time dynamical system. A variety of map formulations are possible in the CRTBP and Hill's problem, including the periapsis map (Villac and Scheeres, 2003; Howell et al., 2011) which will be used later.

The strategy of coupling together a flyby of the Earth and capturing NEAs onto Sun–Earth L_1/L_2 periodic orbits is now proposed. The dynamical model of the CRTBP is firstly introduced to calculate Lyapunov orbits around the Sun-Earth L_1/L_2 points and their associated stable manifolds. Then, according to the height of the flyby orbit at perigee, two types of the Earth flyby are determined, an Earth flyby with and without high altitude aerobraking. A grazing flyby is used, but it is assumed that only small bodies which would safely ablate in the Earth's atmosphere at lower altitudes are considered for aerobraking. After selecting appropriate candidate NEAs and calculating the NEA capture window, a detailed design procedure is presented and finally global optimization is carried out. Meanwhile, the NEA capture strategy without an Earth flyby is investigated and results then obtained. Comparing the results of NEA capture strategies with and without the Earth flyby, the NEA capture strategy using an Earth flyby with and without aerobraking both have the potential to be cheaper. Moreover, these NEA capture strategies using an Earth flyby also have the potential to be save flight time.

2. Dynamical model

2.1 Circular Restricted Three-Body Problem

The Sun and Earth are assumed to be in circular orbits around their common centre–of-mass while the NEA moves under the gravitational attraction of these two primary bodies. In a coordinate frame *xyz* with non-dimensional units which is centred at the Sun-Earth barycentre and rotating synchronously with the primaries, shown in Fig. 1, the Sun and Earth are located at $[-\mu, 0, 0]^T$ and $[1-\mu, 0, 0]^T$, respectively. Therefore, the model of the circular restricted three-body problem (CRTBP) is introduced to describe the motion of an NEA as follows (Szebehely, 1967)

$$\ddot{x} - 2\dot{y} = \frac{\partial \Omega}{\partial x}, \quad \ddot{y} + 2\dot{x} = \frac{\partial \Omega}{\partial y}, \quad \ddot{z} = \frac{\partial \Omega}{\partial z} \tag{1}$$

where

$$\Omega(x, y, z, \mu) = \frac{1}{2}[(x^2 + y^2) + \mu(1-\mu)] + \frac{1-\mu}{r_1} + \frac{\mu}{r_2}$$

and $r_1 = [(x+\mu)^2 + y^2 + z^2]^{1/2}$, $r_2 = [(x-1+\mu)^2 + y^2 + z^2]^{1/2}$ are the distances of the NEA to the two primary bodies and the distance between the Sun and Earth is normalized to 1 (SE unit); $\mu = m_e / (m_s + m_e)$ is the mass parameter in the Sun-Earth CRTBP system and m_s and m_e are the mass of the Sun and Earth, respectively.

The CRTBP system is autonomous and so there exists an integral of motion in the CRTBP, termed the Jacobi constant *J*, as follows

$$2\Omega(x, y, z, \mu) - (\dot{x}^2 + \dot{y}^2 + \dot{z}^2) = J \tag{2}$$

For the CRTBP, there are also five Lagrange points, also known as the libration points, L_i, (i = 1, 2 . . . 5). The mass parameter assumed for this model is $\mu = 3.036 \times 10^{-6}$ (Koon et al., 2011). In this paper, the collinear libration points L_1 and L_2 are the target libration points for the captured NEAs.

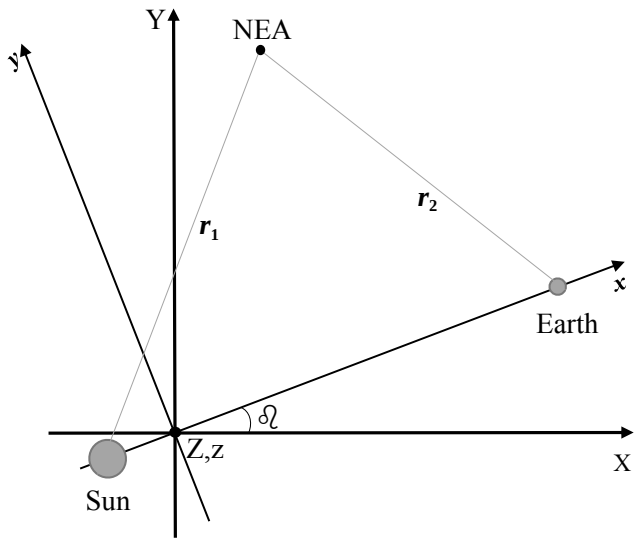

Figure 1. Geometry of the Sun-Earth CRTBP system in the Sun-Earth rotating frame *xyz* and in an inertial frame XYZ

2.2 Lyapunov orbits and invariant manifolds

There exist numerous periodic solutions to the CRTBP problem and so numerical algorithms have been proposed to determine these periodic orbits (Richardson, 1980; Gómez, 2001; Henon, 2003). In this paper, the planar Lyapunov orbits are investigated as the target periodic orbits for the captured NEAs. Families of periodic orbits with different Jacobi constants can be obtained by using differential correction, based on the initial states which are estimated by means of the Richardson third-order approximation (Richardson, 1980), as shown in Fig. 2.

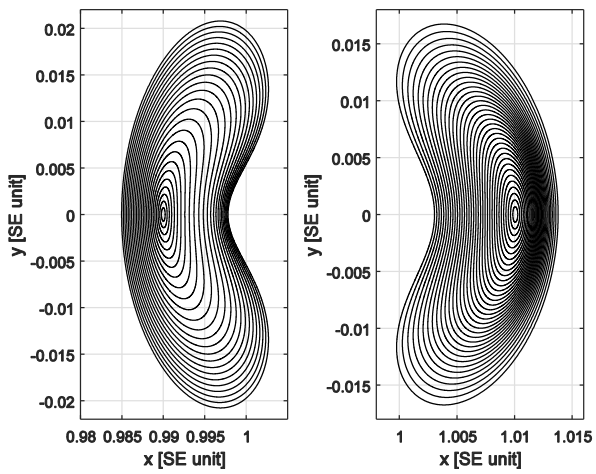

Figure 2. Lyapunov orbits around L_1 (left) with Jacobi constant [3.00008799, 3.00089706] and L_2 (right) with Jacobi constant [3.00023845, 3.00089301] in the Sun-Earth CRTBP system

Lyapunov orbits are unstable periodic orbits which have associated stable manifolds and unstable manifolds. The stable manifolds or unstable manifolds of a periodic orbit are the set of trajectories that asymptotically approach or depart the target orbit and can be calculated under a perturbation in the direction of the stable or unstable eigenvector. The stable manifold W^S consists of the set of all possible trajectories through which a particle could be asymptotically inserted onto the target periodic orbit, corresponding to the stable eigenvector. The stable manifolds associated with a Sun-Earth L_2 Lyapunov orbit are shown in Fig. 3.

A Poincaré map can transform a continuous time dynamical system to a discrete time dynamical system. To obtain the state of the perigee of the Earth flyby orbit, we use the periapsis map as a Poincaré map (Villac and Scheeres, 2003; Howell et al., 2011). The periapsis map is defined by the following condition

$$\dot{r}_2 = 0, \ddot{r}_2 > 0 \tag{3}$$

The periapsis map of the stable manifolds associated with the Sun-Earth L_1/L_2 Lyapunov orbits can be obtained by propagating the stable manifolds backward until they cross the section defined by Eq. (3). An example of the periapsis map of the stable manifolds associated with a Sun-Earth L_2 Lyapunov orbit is shown in Fig. 3. In this paper, the aerobraking manoeuvre, or an additional propulsive manoeuvre, is assumed to occur at the perigee of the Earth flyby orbit where the state of the perigee of the flyby orbit can be determined by the periapsis condition defined by Eq. (3).

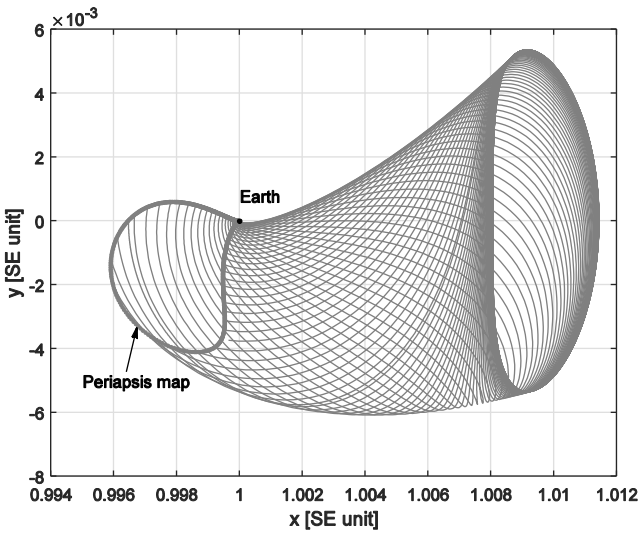

Figure 3. Stable manifolds associated with a Sun-Earth L_2 periodic orbit and the periapsis map

2.3 Coordinate transformation

As shown in Fig. 1, the direction of the Earth with respect to the Sun-Earth barycentre in the inertial frame XYZ is described by the angle β, measured from the x-axis. We denote the states of the Sun-Earth L_1/L_2 stable manifolds at the periapsis map in the Sun-centred inertial frame and in the Sun-Earth rotating frame by $\boldsymbol{S}_S^{in}$ and $\boldsymbol{S}_{SE}^{ro}$ respectively. Thus, we have

$$\boldsymbol{S}_S^{in} = \boldsymbol{R}(\beta)(\boldsymbol{S}_{SE}^{ro} - \boldsymbol{S}_{Sun}), \beta \in [0, 2\pi] \tag{4}$$

$$\boldsymbol{S}_{SE}^{ro} = \boldsymbol{R}^{-1}(\beta)\boldsymbol{S}_S^{in} + \boldsymbol{S}_{Sun}, \beta \in [0, 2\pi] \tag{5}$$

where $\boldsymbol{S}_{Sun} = [-\mu, 0, 0, 0, 0, 0]^T$ and

$$\boldsymbol{R}(\beta) = \begin{bmatrix} \cos\beta & -\sin\beta & 0 & 0 & 0 & 0 \\ \sin\beta & \cos\beta & 0 & 0 & 0 & 0 \\ 0 & 0 & 1 & 0 & 0 & 0 \\ -\sin\beta & -\cos\beta & 0 & \cos\beta & -\sin\beta & 0 \\ \cos\beta & -\sin\beta & 0 & \sin\beta & \cos\beta & 0 \\ 0 & 0 & 0 & 0 & 0 & 1 \end{bmatrix} \tag{6}$$

In the following sections, Eq. (4) will be used to transform the state of the candidate NEA in the Sun-centred inertial frame to the Sun-Earth rotating frame. Moreover, Eq. (5) will be used to transform the state of the NEA at the aerobraking manoeuvre in the Earth-centred inertial frame to the Sun-Earth rotating frame. Consequently, the dynamical model of the aerobraking manoeuvre in the Sun-Earth rotating frame can be obtained.

3. Strategies for Earth flyby

During the flyby of the Earth, the Earth's atmosphere may provide opportunities for a grazing aerobraking manoeuvre to move the NEA onto the stable manifold of the Sun-Earth L_1 or L_2 periodic orbits. However, issues associated with the precision of the aerobraking required for subsequent injection onto the stable manifold are not considered here. However, for a small NEA the body may in principle be actively guided by a carrier spacecraft (Brophy et al., 2012), with the carrier spacecraft remaining attached to, and shielded, by the NEA during the aerobraking manoeuvre. Therefore, there will exist two types of Earth flyby, i.e. with and without the aerobraking manoeuvre, corresponding to a low or high altitude flyby orbit at perigee. In practice only small bodies would be considered to mitigate impact risks and so we envisage targeting NEAs which would

completely ablate in the Earth's atmosphere at low altitude in the event of a failure prior to or during the aerobraking pass (Vasile and Colombo, 2008).

The trajectory of the captured NEA in the Earth's atmosphere can be modelled by means of a Keplerian orbit. Thus, assuming that the NEA remains in the Earth's atmosphere for a small arc of true anomaly close to pericentre and the ablative mass loss of the NEA is small, an approximation for the $\Delta \boldsymbol{v}$ imparted to the NEA through aerobraking can be obtained. The model assumes an exponential atmospheric model and quadratic drag as developed by (Heppenheimer, 1971; Sanchez and McInnes, 2012) and used by (Heppenheimer, 1971; Sanchez and McInnes, 2012) such that

$$\Delta \boldsymbol{v} = (1 - e^{B\rho\sqrt{2\pi r_p H_s (e+1)/e}})\boldsymbol{v}_p \tag{7}$$

where $\boldsymbol{v}_p$ is the relative velocity of the NEA at perigee with respect to the Earth and

$$B = C_d \frac{A}{2M} \tag{8}$$

is the NEA ballistic coefficient, where C_d is the drag coefficient of a sphere, assumed to be 0.47 (Sanchez and McInnes, 2012); A/M is the area-to-mass ratio of the NEA; r_p is the perigee radius of the flyby orbit from the centre of the Earth and e is the eccentricity of the flyby orbit; H_s is the atmosphere scale height. Assuming that the NEA is a spherical with density ρ_a = 2600 kg/m^3 (Chesley et al., 2002), the NEA ballistic coefficient can be written as

$$B = 0.75 C_d \frac{1}{D\rho} \tag{9}$$

where D is the diameter of the NEA.

Many density models of the Earth's atmosphere have been developed, including the Standard Atmosphere, USSA76 and COSPAR International Reference Atmosphere. However, one of the simplest models is the exponential atmospheric model (Vallado, 2007). In this model, it is assumed that the density of the atmosphere deceases exponentially from the Earth's surface and so can be written as

$$\rho = \rho_0 e^{-\frac{h}{H_s}} \tag{10}$$

where ρ_0 = 1.225 kg/m^3 is the density of the Earth's atmosphere at the surface and H_s = 7.249 km is the scale height (Vallado, 2007).

From Fig. 4, we note that once the height h at perigee above the Earth's surface is larger than approximately 100 km, the Earth's atmosphere can be assumed not to provide an aerobraking manoeuvre. Therefore, we define $h_{threshold}$ = 100 km as the height threshold for aerobraking, or $r_{threshold}$ = 6478 km (r_{Earth} + 100 km) as the distance threshold for aerobraking, where r_{Earth} = 6378 km is the radius of the Earth.

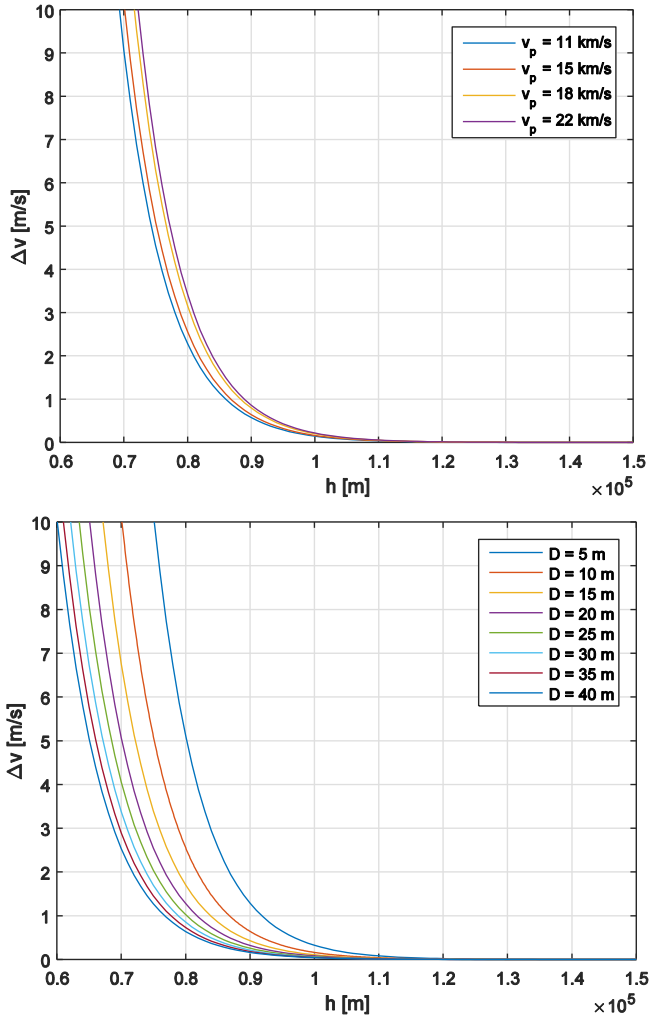

Figure 4. (a) Aerobraking Δv provided by the atmosphere as a function of height h and different relative velocities v_p of the NEA, given a NEA diameter of D = 10 m; (b) Aerobraking Δv provided by the atmosphere as a function of height h and NEA diameter D given a perigee speed v_p = 15 km/s.

4. NEA capture opportunities

4.1 Candidate NEA selection

To obtain possible capture opportunities for NEAs, the JPL Small Body Database[2] is used. This database represents the current catalogued NEAs, including their orbital elements and estimated size.

To capture NEAs with low energy, it is necessary to remove those NEAs with a high inclination and a semi-major axis far from that of the Earth's. Therefore, those NEAs with

[2] https://ssd.jpl.nasa.gov/?sb_elem

a semi-major axis in the range 0.85-1.15 AU are considered to be candidates which can be captured into the vicinity of the Earth with a relatively low energy (Sanchez et al., 2012). Furthermore, the Jacobi constant J of the NEA can be approximated by the Tisserand parameter as follows

$$J \approx \frac{1}{a} + 2\sqrt{a(1-e^2)\cos i} \tag{11}$$

where a, e and i are the semi-major axis (in AU), eccentricity and inclination of the NEA orbit. If an NEA's Jacobi constant is significantly different from that of the final periodic orbit, it may have too high a total cost for capture (Sánchez and Yárnoz, 2016). It should therefore be possible to achieve low energy capture with a Jacobi constant close to the Jacobi constant of the target periodic orbit. Therefore, here we set $J = 2.99$ as the critical value. Those NEAs with $J \geq 2.99$ are then considered to be candidate NEAs.

However, a captured NEA using an Earth flyby may present a collision risk, as noted above. Therefore, we only consider those NEAs with a diameter less than 40 m since this is considered to be the critical threshold above which the Earth's atmosphere will no longer disintegrate a NEA (Vasile and Colombo, 2008). Here it is assumed that the NEA is a homogeneous spherical object with density ρ_a and diameter D. The diameter D of the NEA can be estimated by the following relationship (Chesley et al., 2002)

$$D = 1329\text{km} \times 10^{-H/5} p_v^{-1/2} \tag{12}$$

where H is absolute magnitude of the NEA and p_v is its albedo. Here we assume that the NEAs are typical and thus have a density $\rho_a = 2600$ kg/m^3 and albedo $p_v = 0.154$ (Chesley et al., 2002). If $D \leq 40$ m then $H \geq 24.64$. Considering the filters stated above, the candidate NEAs should be those NEAs with $H \geq 24.64$, $J \geq 2.99$ and $a \in [0.85, 1.15]$, as shown in Fig. 5.

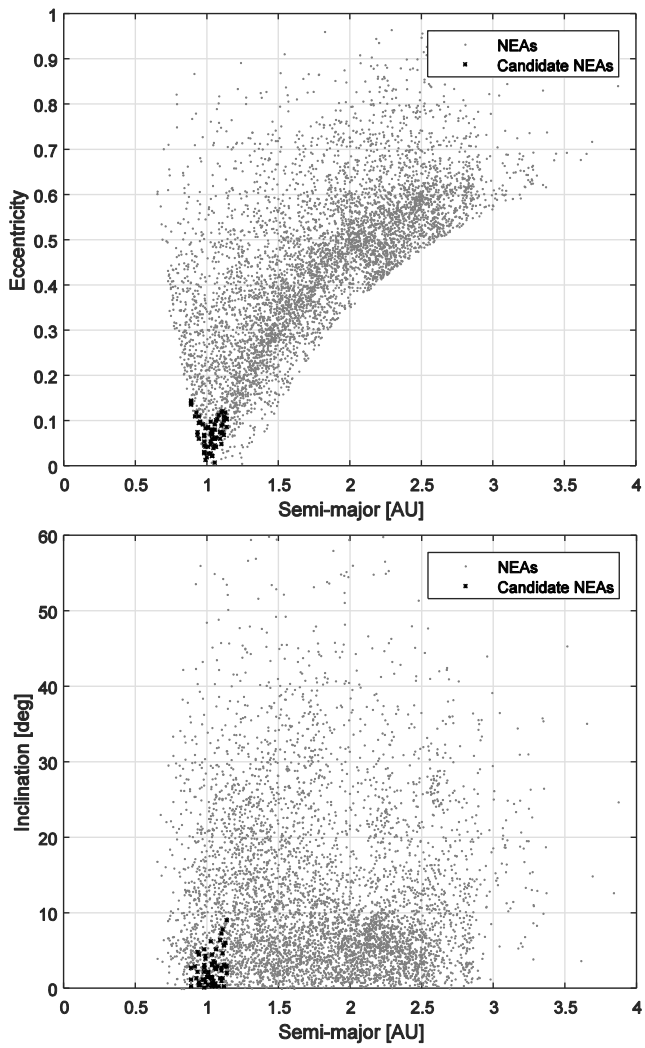

Figure 5. Distribution of candidate NEAs

4.2 NEA capture window

For each of these candidate NEAs, feasible capture dates are assumed to be in the interval 2018–2050 (or 58119 MJD - 70171 MJD). It is assumed that the NEA orbital elements remain unchanged until they have a close approach to the Earth. We define this time period during which the NEA orbital elements are valid as the NEA capture window. In this paper, it is assumed that the upper limit of the NEA capture window is the date when the distance of the candidate NEA to the Earth is 0.21 AU where the gravitational attraction of the Earth is then considered small enough with respect to the gravity of the Sun (the ratio of Earth's and Sun's gravity is then less than 10^{-4}). Denoting the date when the NEA has a distance to the Earth of 0.21 AU as $T_{threshold}$ ($T_{threshold} \leq 2050$), the capture window of a candidate NEA is then $[2018, T_{threshold}]$, shown in Fig. 6.

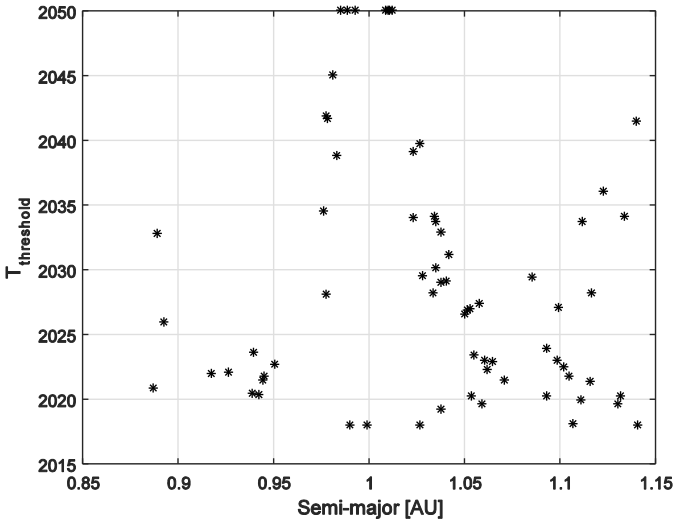

Figure 6. $T_{threshold}$ of candidate NEAs

5. NEA capture using Earth flyby without aerobraking

5.1 Problem statement

In this capture strategy, a flyby of the Earth without aerobraking is used. The candidate NEA leaves its orbit with an impulse manoeuvre and approaches the vicinity of the Earth for the flyby. At the perigee of the flyby, an additional manoeuvre is imposed on the candidate NEA. This is because a manoeuvre at perigee can represent the most effective way to achieve the outgoing flyby orbit (Ceriotti, 2010). Finally, the NEA moves onto the stable manifold of a target periodic orbit around the Sun-Earth L_1 or L_2 points and will be asymptotically captured onto it. In this scenario, a manoeuvring spacecraft is first assumed to be attached to the target NEA before the first manoeuvre and will then stay attached to the NEA for the entire mission. All the propulsive manoeuvres will be provided by the manoeuvring spacecraft. It should be noted that the entire transfer trajectory is modelled in the Sun-Earth CRTBP.

Figure 7 shows a schematic of the NEA capture strategy using an Earth flyby without aerobraking. The basic concept of the NEA capture strategy is though the following steps:

(1) With an initial manoeuvre $\Delta\boldsymbol{v}_1$, the candidate NEA leaves its initial orbit and its motion can then be described by the Sun-Earth CRTBP, shown in Fig. 7(a);

(2) With a second manoeuvre $\Delta\boldsymbol{v}_2$, the NEA approaches the vicinity of the Earth and then reaches perigee, shown in Fig. 7(b);

(3) At the perigee, a third manoeuvre $\Delta \boldsymbol{v}_3$, which is parallel to the NEA's current velocity vector, is applied to the NEA and the NEA then moves onto the stable manifold of a Sun-Earth L_1 or L_2 periodic orbit and so will asymptotically transfer onto it, shown in Fig. 7(b).

The total cost of capturing an NEA onto the target periodic orbit around the Sun-Earth L_1 or L_2 points can then be written as

$$\Delta v = \|\Delta \boldsymbol{v}_1\| + \|\Delta \boldsymbol{v}_2\| + \|\Delta \boldsymbol{v}_3\| \tag{13}$$

Therefore, for each candidate NEA, six parameters can determine the NEA capture manoeuvre using an Earth flyby without aerobraking, as defined in Fig. 7 and described as follows: (1) epoch T_0 when the first manoeuvre is applied to the candidate NEA; (2) flight time T_{fly1} between the first manoeuvre and the second manoeuvre; (3) flight time T_{fly2} between the second manoeuvre and the third manoeuvre; (4) Jacobi constant J of the target Sun-Earth L_1 or L_2 Lyapunov orbit; (5) time t_p determining the point along the Lyapunov orbit where the stable manifold of the target Lyapunov orbit is propagated backward from and where $t_p \in [0\ T_p]$ where T_p is the period of the final target orbit; (6) third manoeuvre Δv_3 that is parallel to the velocity vector of the NEA at the perigee.

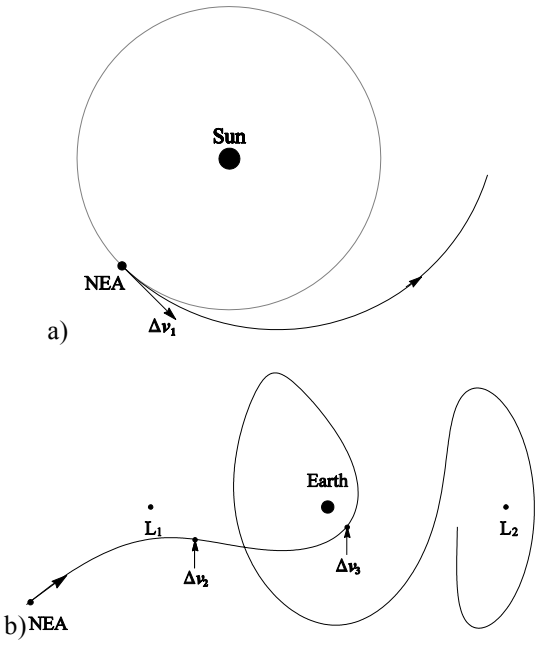

Figure 7. Schematic strategy for NEA capture using Earth flyby without aerobraking

5.2 Differential correction

A differential correction method will be utilized to design the transfer trajectory between the candidate NEA's initial orbit and the target point on the stable manifold

associated with the Sun-Earth LPOs in the following section. It is assumed that the NEA initial state is $\boldsymbol{S_i} = [x_i, y_i, z_i, \dot{x}_i, \dot{y}_i, \dot{z}_i]^T$ and then the final state after flight time T is $\boldsymbol{S}'_f = [x'_f, y'_f, z'_f, \dot{x}_f, \dot{y}_f, \dot{z}_f]^T$ Assuming that the state of the target point is $\boldsymbol{S_f} = [x_f, y_f, z_f, \dot{x}_f, \dot{y}_f, \dot{z}_f]^T$, we can then seek conditions such that $\delta \boldsymbol{S_f} = [\delta x_f, \delta y_f, \delta z_f, 0, 0, 0]^T = [x_f - x'_f, y_f - y'_f, z_f - z'_f, 0, 0, 0]^T = \mathbf{0}$ by correcting the initial velocity vector $\delta \boldsymbol{S_i} = [0, 0, 0, \delta \dot{x}_i, \delta \dot{y}_i, \delta \dot{z}_i]^T$ as follows

$$\delta \boldsymbol{S_i} = \Phi^{-1} \delta \boldsymbol{S_f} \tag{14}$$

where Φ is the 6×6 state transition matrix of the CRTBP.

A heliocentric Sun-centered two-body Lambert arc with two impulsive manoeuvres can be used to provide an initial guess, where the first impulse is applied and the asteroid transfers to the Sun-Earth stable manifolds. The differential correction defined by Eq. (14) uses this initial guess and then the correction is repeated until $\delta \boldsymbol{r_f} = [\delta x_f, \delta y_f, \delta z_f]^T$ approaches **0**, within some small tolerance.

5.3 Design Procedure

The process of designing the transfer trajectory to capture the candidate NEA using an Earth flyby without aerobraking is as follows:

(1) Select one target NEA in the candidate catalogue (e.g. 2010UJ) in Fig. 5;

(2) Given the Jacobi constant J and the parameter t_p, the stable manifold associated with the final periodic orbit is propagated backward with a given propagation time (e.g. 200 days); the perigee where the third manoeuvre Δv_3 is applied to the NEA can then be determined, corresponding to the perigee along the stable manifold with the closest distance to the Earth and a height above the Earth's surface larger than 100 km. Then, the state $\boldsymbol{S_{p+}} = [x_p, y_p, z_p, \dot{x}_p, \dot{y}_p, \dot{z}_p]^T$ at perigee is obtained, shown in Fig. 8;

(3) Given the value of the third manoeuvre Δv_3 at perigee, the state before the third manoeuvre is $\boldsymbol{S_{p-}} = [x_p, y_p, z_p, \lambda \dot{x}_p, \lambda \dot{y}_p, \lambda \dot{z}_p]^T$ where $\lambda = 1 + \Delta v_3 / (\dot{x}_p^2 + \dot{y}_p^2 + \dot{z}_p^2)^{1/2}$;

(4) Given the flight time T_{fly2}, the state $\boldsymbol{S_{p-}}$ is propagated backward and then the target point $\boldsymbol{S_f}$ is obtained, shown in Fig. 9;

(5) Given a departure date T_0, the transformation of the initial state of the candidate NEA in the Sun-centred inertial frame to the Sun-Earth rotating frame $\boldsymbol{S_i}$ is then obtained;

(6) Given the flight time T_{fly1}, the Lambert arc in the Sun-centered two-body problem is utilized to design the transfer to the stable manifold from the candidate asteroid's orbit and

so the first impulse can be estimated; based on the initial guess of the first impulse, the differential correction method in Eq. (14) is then applied to design the transfer between the candidates NEA's initial orbit $\boldsymbol{S}_i$ and the target point $\boldsymbol{S}_f$. Thus, the manoeuvres Δv_1 and Δv_2 can be calculated.

The total cost of capturing the NEA onto a Sun-Earth L_1/L_2 periodic orbit using the Earth flyby can then be obtained, where the entire transfer trajectory is shown in Fig. 10 and Fig. 11.

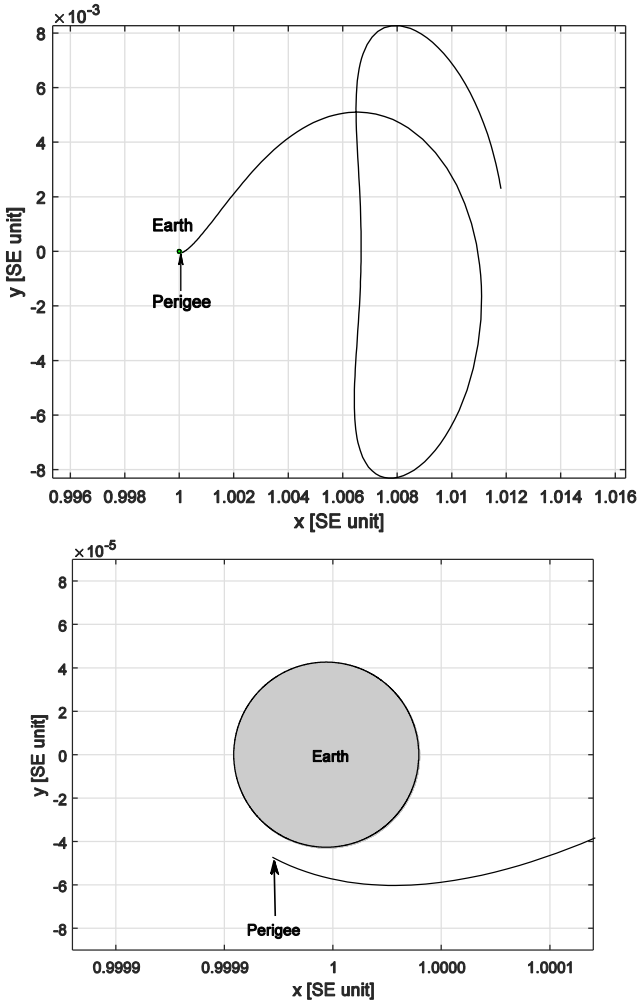

Figure 8. Given C=3.00079405, t_p=1.575712, perigee of the stable manifold associated with the Sun-Earth L_2 Lyapunov orbit

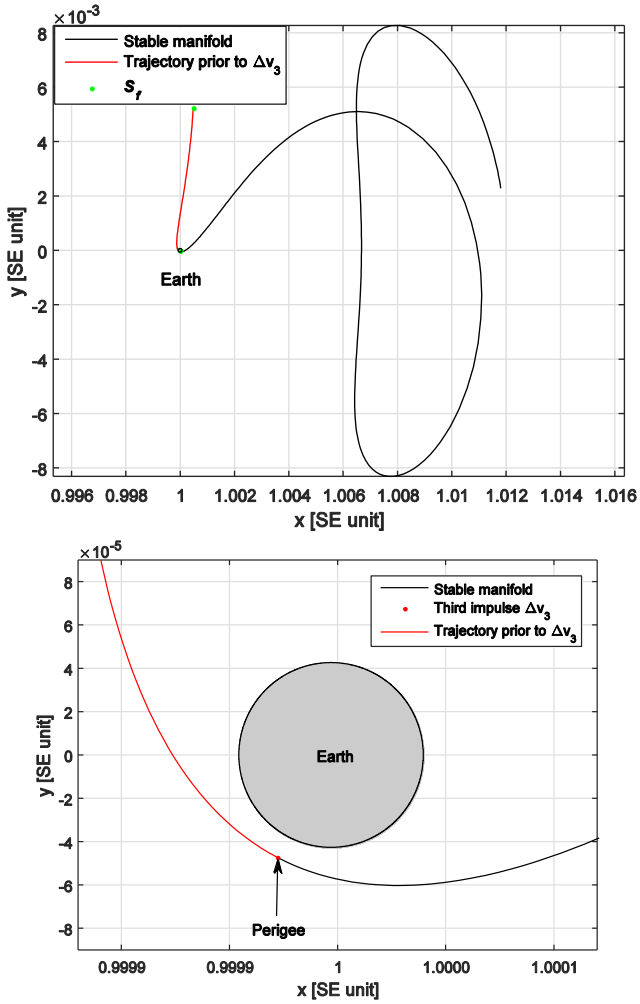

Figure 9. Given $\Delta v_3 = 0.005194$ and $T_{fly2} = 0.322368$, the trajectory prior to Δv_3 is obtained by propagating backward from the state at perigee.

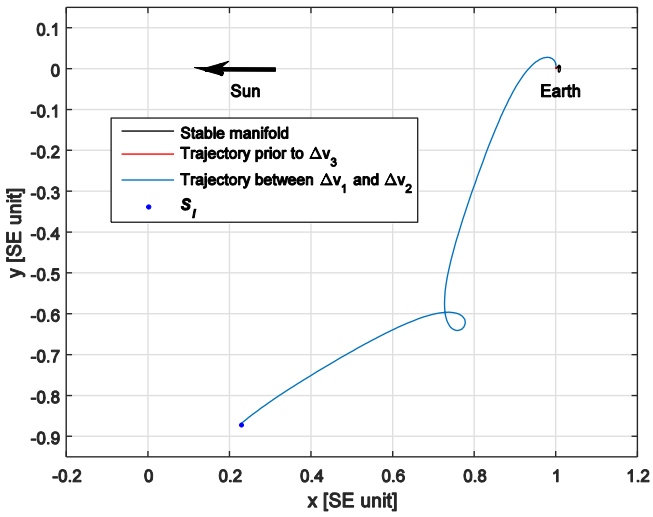

Figure 10. Given $T_0 = 59287.2$ [MJD], $T_{fly1} = 4.134983$, the transfer trajectory (xy projection) to capture 2010UJ onto a Sun-Earth L_2 Lyapunov orbit in the Sun-Earth rotating frame.

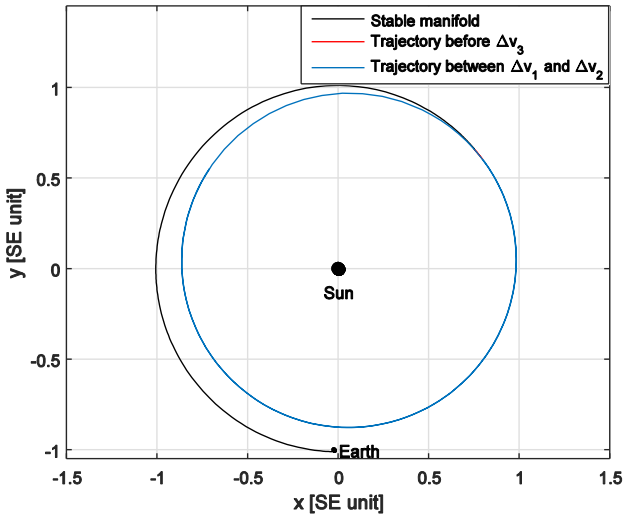

Figure 11. Transfer trajectory (*xy* projection) for capturing 2010UJ onto the Sun-Earth L_2 Lyapunov orbit in the Sun-centred inertial frame.

5.4 Optimization

For each of these candidate NEAs, feasible capture transfers with capture dates in the interval 2018–$T_{threshold}$ were obtained. Then, for each candidate NEA, there are 6 parameters, so the problem can be defined with the following variables: departure date T_0, flight time T_{fly1}, flight time T_{fly2}, the Jacobi constant J of the target Lyapunov orbit, a variable t_p associated with the state on the target orbit where the stable manifold is integrated from and the value of the third manoeuvre Δv_3 that is parallel to the velocity vector of the NEA at perigee of the flyby orbit. As the objective function for this optimization problem, the total cost Δv can be minimised by optimizing over these 6 parameters (T_0, T_{fly1}, T_{fly2}, J, t_p, Δv_3) using NSGA-II, a global optimisation method that uses a non-dominated sorting-based multi-objective evolutionary algorithm (Deb et al., 2002). Then transfers obtained with NSGA-II can be locally optimized with sequential quadratic programming (SQP), implemented in the function *fmincon* in MATLAB. The optimal results of NEA capture using the Earth flyby without aerobraking are shown in Table 1.

Table 1 Results of capturing NEAs onto Sun-Earth L_1/L_2 Lyapunov orbits using an Earth flyby without aerobraking

NEA	Total cost, m/s	Epoch, MJD	Total flight time, days	Jacobi constant of Lyapunov orbit	Propellant mass, ton	Target point
2003WT153	843.07	58638.9	365.5	3.00080233	205.3	L_2
2006UQ216	1217.8	61686.1	860.1	3.00009708	735.4	L_1

2007UN12	193.64	58297.1	1595.7	3.00008893	19.9	L_1
2008EL68	492.65	58393.8	1209.0	3.00038241	192.1	L_1
2008JL24	793.05	58646.5	2148.1	3.00015052	21.3	L_1
2009YR	996.75	58168.2	1132.9	3.00052577	236.9	L_1
2009YR	881.13	58274.6	841.6	3.00031693	213.3	L_2
2010UJ	574.36	59036.2	622.1	3.00052358	1755.6	L_1
2010UJ	515.71	59287.2	464.5	3.00079405	1591.3	L_2
2010UY7	747.02	61556.4	459.6	3.00039055	92.6	L_2
2010VQ	820.62	58257.6	401.7	3.00076975	303.6	L_2
2011BQ50	553.99	58918.9	1174.8	3.00052923	141.3	L_1
2011CL50	440.14	58706.2	808.2	3.00038285	198.7	L_2
2012HG2	484.67	60448.8	791.8	3.00008868	497.7	L_1
2012WR10	661.51	61424.2	1062.9	3.00070261	63.0	L_1
2014JR24	889.81	58716.7	2569.3	3.00017493	35.7	L_1
2014QN266	574.78	61256.2	1070.1	3.00014755	1530.1	L_1
2014QN266	668.90	61271.3	518.0	3.00053956	1753.8	L_2
2015PS228	698.47	62932.5	1554.4	3.00015471	47.5	L_1

5.5 Comparison of the results of NEA capture with and without Earth flyby

According to the work of Yárnoz et al. (2013) and Sánchez and Yárnoz (2016), a candidate NEA can be captured directly from its orbit to the stable manifold of the target Sun-Earth L_1/L_2 periodic orbit. The candidate NEA is first assumed to leave its orbit with an initial manoeuvre and then will move onto the stable manifold of the Sun-Earth L_1/L_2 periodic orbit with a second manoeuvre. These two manoeuvres can be calculated by solving a Lambert arc between the NEA orbit and the stable manifold in the Sun-inertial two-body problem. Finally, once the NEA moves onto the stable manifold, it will then transfer to the target periodic orbit without any further manoeuvres. In this work, to avoid too long a flight time for capturing the NEAs, Lambert arcs with up to 2 complete revolutions from the NEA initial orbit to the stable manifold are considered. The schematic diagram of the NEA capture strategy without Earth flyby is shown in Fig. 12. In this NEA capture strategy, there are 5 parameters: departure date T_0, flight time T_{fly1} between the asteroid's orbit and the stable manifold, stable manifold transfer time T_{fly2}, the

Jacobi constant J of the target Lyapunov orbit, a variable t_p associated with the state on the target orbit where the stable manifold is integrated from. Then the total Δv can be minimised by optimizing over these 5 parameters using NSGA-II. Then transfers obtained with NSGA-II can be locally optimized with a gradient-based method, such as the SQP implemented in the function *fmincon* in MATLAB. The optimal results of NEA capture using the Earth flyby without aerobraking are shown in Table 1. Therefore, the optimal results of NEA capture without Earth flyby are also listed in Table 2.

Comparing the results of Table 1 and Table 2, we can note that the NEA capture strategy using an Earth flyby has the potential to be cheaper in terms of Δv than the capture strategy without the Earth flyby, especially for 2003WT153, 2011CL50 and 2012HG2, et al. Moreover, since NEA capture using an Earth flyby does not require significantly more time for the captured NEA to travel along the stable manifold of the Sun-Earth L_1/L_2 periodic orbit, this capture strategy also has the potential to achieve quicker transfers, e.g. 2003WT153, 2010UJ and 2011CL50, et al. Moreover, some candidate NEAs can be simultaneously captured with low energy onto periodic orbits both around the Sun-Earth L_1 and L_2 points, e.g. 2009YR, 2010UJ and 2014QN266 et al. Therefore, the Earth flyby can be regarded as a way of increasing NEA capture opportunities. However, one drawback of the NEA capture strategy using an Earth flyby is that the NEA flies by the Earth at a relatively high velocity and thus we have limited time to apply the third manoeuvre to the NEA at the perigee of the flyby orbit. Therefore, in principle a high thrust engine would be required to achieve the third manoeuvre in a realistic mission scenario.

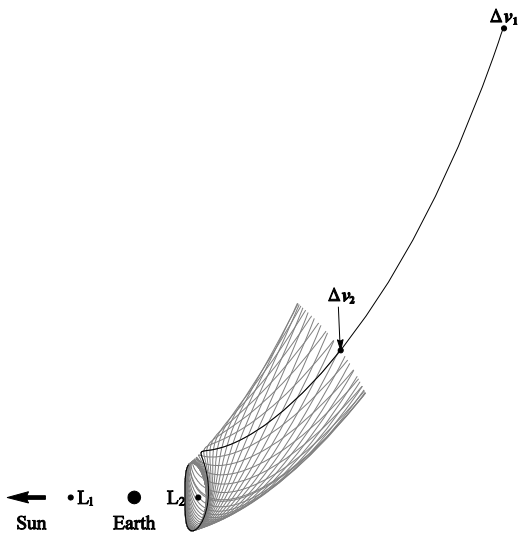

Fig. 12 Schematic strategy for NEA capture without Earth flyby

Table 2 Results of capturing NEAs onto Sun-Earth L_1/L_2 Lyapunov orbits without using an Earth flyby

NEA	Total cost, m/s	Epoch, MJD	Total flight time, days	Jacobi constant of Lyapunov orbit	Propellant mass, ton	Target point
2003WT153	2049.47	58151.6	2005.7	3.00013872	414.8	L_1
2006UQ216	1757.21	61469.4	967.7	3.00061006	977.2	L_2
2007UN12	303.06	58580.8	756.4	3.00061320	30.6	L_2
2008EL68	818.07	62673.9	2670.3	3.00064089	302.7	L_2
2008JL24	968.78	58705.2	1974.5	3.00030555	25.4	L_2
2008UA202	470.55	59889.3	1618	3.00053193	17.6	L_2
2009YR	1063.19	58120.8	1494.0	3.00012440	250.1	L_1
2010JR34	1589.32	58164.6	1549.4	3.00014389	521.7	L_1
2010UJ	750.47	58462.0	1549.8	3.00039880	2229.9	L_1
2010UY7	1541.23	58939.0	1778.9	3.00013998	168.7	L_1
2010VQ	2351.54	58135.3	1497.0	3.00031707	689.2	L_1
2011BQ50	699.46	58925.1	1546.0	3.00028523	174.3	L_1
2011CL50	1502.87	58634.5	1715.3	3.00036376	573.9	L_1
2012HG2	1824.27	59032.1	2351.3	3.00045694	1520.1	L_2
2012WR10	902.13	60917.6	1839.5	3.00025078	82.7	L_2
2014AA	2926.1	58402.0	2274.7	3.00034024	9.5	L_2
2014JR24	1260.13	59417.2	1386.6	3.00028684	47.7	L_2
2014QN266	671.63	60136.6	1395.7	3.00033712	1760.2	L_2
2014UV210	1450.96	58490.5	1462.8	3.00030621	1468.9	L_2
2014WE6	1446.04	62447.9	1629.8	3.00010017	11.6	L_1
2014WX202	400.69	61416.5	2174.9	3.00031213	11.5	L_2
2015PS228	709.89	60891.8	1973.2	3.00041603	48.2	L_2

6. NEAs capture using aerobraking

In this capture strategy using aerobraking, the candidate NEA is firstly assumed to leave its orbit with an impulse manoeuvre and approach the vicinity of the Earth for a single aerobraking pass. During the flyby of the Earth, the Earth's atmosphere provides

drag to modify the NEA orbit without the use of propellant. Again, after the flyby of the Earth, the candidate NEA moves onto the stable manifold of a periodic orbit around the Sun-Earth L_1 or L_2 points.

6.1 Problem statement

Figure 13 shows the new concept of NEA capture using aerobraking as follows:

(1) With a first manoeuvre $\Delta\boldsymbol{v}_1$, the candidate NEA departs from its initial orbit and its motion can be described by the Sun-Earth CRTBP, shown in Fig. 13(a);

(2) With a second manoeuvre $\Delta\boldsymbol{v}_2$, the NEA approaches the vicinity of the Earth and accordingly it reaches perigee;

(3) An aerobraking manoeuvre is applied to the candidate NEA and then the NEA moves onto the stable manifold of a Lyapunov orbit around the Sun-Earth L_1 or L_2 points and will finally be captured, shown in Fig. 13(b).

The total cost of capturing the candidate NEA onto the target periodic orbit around the Sun-Earth L_1 or L_2 points can then be written as

$$\Delta v = \|\Delta\boldsymbol{v}_1\| + \|\Delta\boldsymbol{v}_2\| \tag{15}$$

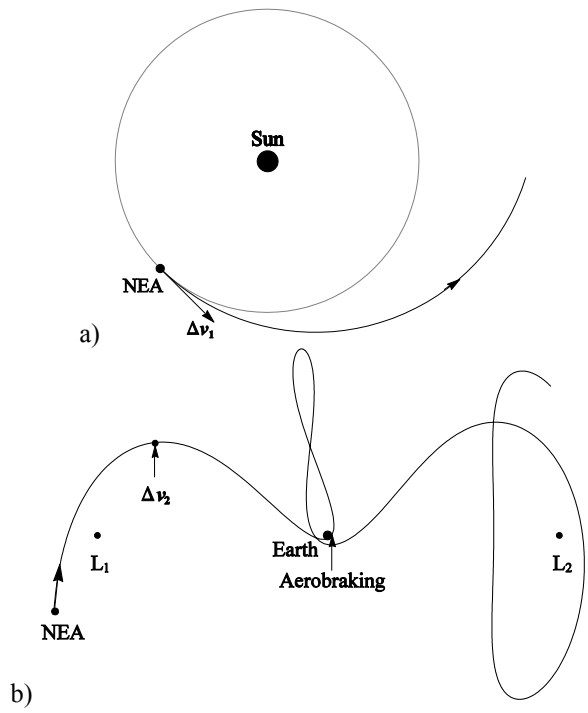

Figure 13. Schematic strategy for NEA capture using aerobraking

Hence, for each candidate NEA, there now are 5 parameters to describe the sequence of manoeuvres as follows: (1) epoch T_0 when the NEA departs from its initial orbit; (2) flight

time T_{fly1} between the first manoeuvre and the second manoeuvre; (3) flight time T_{fly2} between the second manoeuvre and the aerobraking phase; (4) Jacobi constant J of the final Lyapunov orbit around the Sun-Earth L_1 or L_2 points; (5) time t_p associated with the point on the periodic orbit where the stable manifold is integrated from where $t_p \in [0\ T_p]$, where T_p is the period of the final Lyapunov orbit.

6.2 Aerobraking phase

Assuming that the states of the candidate NEA before and after aerobraking in the Earth-centred inertial frame are given by $\boldsymbol{S}_{p-}^{E} = [x_p^E, y_p^E, z_p^E, \dot{x}_{p-}^E, \dot{y}_{p-}^E, \dot{z}_{p-}^E]^T$ and $\boldsymbol{S}_{p+}^{E} = [x_p^E, y_p^E, z_p^E, \dot{x}_{p+}^E, \dot{y}_{p+}^E, \dot{z}_{p+}^E]^T$, respectively, then Eq. (7) can be written as

$$\frac{\boldsymbol{V}_{p+}}{\boldsymbol{V}_{p-}} = e^{-B\rho\sqrt{2\pi r_p H_s (e_- + 1)/e_-}} \tag{16}$$

$$\boldsymbol{r}_{p+} = \boldsymbol{r}_{p-} \tag{17}$$

where $\boldsymbol{V}_{p-} = [\dot{x}_{p-}^E, \dot{y}_{p-}^E, \dot{z}_{p-}^E]^T$, $\boldsymbol{V}_{p+} = [\dot{x}_{p+}^E, \dot{y}_{p+}^E, \dot{z}_{p+}^E]^T$, $\boldsymbol{r}_{p-} = [x_p^E, y_p^E, z_p^E]^T$, $\boldsymbol{r}_{p+} = [x_p^E, y_p^E, z_p^E]^T$ and e_- is the eccentricity of the flyby orbit before aerobraking.

Here we assume that aerobraking only provides a limited manoeuvre and thus $e_- \approx e_+$ where e_+ is the eccentricity of the flyby orbit after aerobraking. Therefore, the velocity before aerobraking can be guessed as

$$\boldsymbol{V}_{p-} \approx e^{B\rho\sqrt{2\pi r_p H_s (e_+ + 1)/e_+}} \boldsymbol{V}_{p+} \tag{18}$$

The accurate value of the velocity $\boldsymbol{V}_{p-}$ before aerobraking can then be obtained through Newton's method based on the initial guess in Eq. (18).

It is assumed that the states of the candidate NEA before and after aerobraking in the Sun-Earth rotating frame are then $\boldsymbol{S}_{p-} = [x_p, y_p, z_p, \dot{x}_{p-}, \dot{y}_{p-}, \dot{z}_{p-}]^T$ and $\boldsymbol{S}_{p+} = [x_p, y_p, z_p, \dot{x}_{p+}, \dot{y}_{p+}, \dot{z}_{p+}]^T$, respectively. Thus, it can be seen that

$$\begin{aligned} \boldsymbol{V}_{p+} &= \mathbf{K}\boldsymbol{R}(\beta)(\boldsymbol{S}_{p+} - \boldsymbol{S}_{Earth}) \\ \boldsymbol{V}_{p-} &= \mathbf{K}\boldsymbol{R}(\beta)(\boldsymbol{S}_{p-} - \boldsymbol{S}_{Earth}) \end{aligned} \tag{19}$$

where $\boldsymbol{R}(\beta)$ is a coordinate transformation matrix in Section 3.2 and

$$\boldsymbol{S}_{Earth} = [1-\mu, 0, 0, 0, 0, 0]^T, \mathbf{K} = \begin{bmatrix} 0 & 0 & 0 & 1 & 0 & 0 \\ 0 & 0 & 0 & 0 & 1 & 0 \\ 0 & 0 & 0 & 0 & 0 & 1 \end{bmatrix} \tag{20}$$

Defining $\gamma = e^{-B\rho\sqrt{2\pi r_p H_s (e_- + 1)/e_-}}$, Eq. (19) can be written as

$$\mathbf{K}\boldsymbol{R}(\beta)(\boldsymbol{S}_{p-} - \boldsymbol{S}_{Earth}) = \gamma \mathbf{K}\boldsymbol{R}(\beta)(\boldsymbol{S}_{p+} - \boldsymbol{S}_{Earth}) \tag{21}$$

Then,

$$\boldsymbol{R}^{-1}(\beta)\mathbf{K}\mathbf{K}^T\boldsymbol{R}(\beta)(\boldsymbol{S}_{p-} - \boldsymbol{S}_{Earth}) = \gamma \boldsymbol{R}^{-1}(\beta)\mathbf{K}\mathbf{K}^T\boldsymbol{R}(\beta)(\boldsymbol{S}_{p+} - \boldsymbol{S}_{Earth}) \tag{22}$$

Letting $\mathbf{M} = \boldsymbol{R}^{-1}(\beta)\mathbf{K}\mathbf{K}^T\boldsymbol{R}(\beta)$, Eq. (22) can be written as

$$\mathbf{M}(\boldsymbol{S}_{p-} - \boldsymbol{S}_{Earth}) = \gamma \mathbf{M}(\boldsymbol{S}_{p+} - \boldsymbol{S}_{Earth}) \tag{23}$$

where

$$\mathbf{M} = \begin{bmatrix} 0 & 0 & 0 & 0 & 0 & 0 \\ 0 & 0 & 0 & 0 & 0 & 0 \\ 0 & 0 & 0 & 0 & 0 & 0 \\ 0 & -1 & 0 & 1 & 0 & 0 \\ 1 & 0 & 0 & 0 & 1 & 0 \\ 0 & 0 & 0 & 0 & 0 & 1 \end{bmatrix}$$

Hence, Eq. (17) and Eq. (23) can be combined together as follows,

$$\mathbf{M}_1(\boldsymbol{S}_{p-} - \boldsymbol{S}_{Earth}) = \mathbf{M}_2(\boldsymbol{S}_{p+} - \boldsymbol{S}_{Earth}) \tag{24}$$

Thus, we have

$$\boldsymbol{X}_{p-} = \mathbf{M}_1^{-1}\mathbf{M}_2(\boldsymbol{S}_{p+} - \boldsymbol{S}_{Earth}) + \boldsymbol{S}_{Earth} \tag{25}$$

where

$$\mathbf{M}_1 = \begin{bmatrix} 1 & 0 & 0 & 0 & 0 & 0 \\ 0 & 1 & 0 & 0 & 0 & 0 \\ 0 & 0 & 1 & 0 & 0 & 0 \\ 0 & -1 & 0 & 1 & 0 & 0 \\ 1 & 0 & 0 & 0 & 1 & 0 \\ 0 & 0 & 0 & 0 & 0 & 1 \end{bmatrix}, \mathbf{M}_2 = \begin{bmatrix} 1 & 0 & 0 & 0 & 0 & 0 \\ 0 & 1 & 0 & 0 & 0 & 0 \\ 0 & 0 & 1 & 0 & 0 & 0 \\ 0 & -\gamma & 0 & \gamma & 0 & 0 \\ \gamma & 0 & 0 & 0 & \gamma & 0 \\ 0 & 0 & 0 & 0 & 0 & \gamma \end{bmatrix}$$

Therefore, the state of the captured NEA at perigee before the aerobraking phase in the Sun-Earth rotating frame can be estimated by the state of the NEA after aerobraking in the Sun-Earth rotating frame using the Eq. (25).

6.3 Aerobraking window

As noted earlier, the Earth's atmosphere can provide an aerobraking manoeuvre only when the height of the perigee of the flyby orbit is low enough ($h_{threshold}$ = 100 km or $r_{threshold}$ = 6478 km). However, for a Lyapunov orbit, only a few stable manifolds can meet such a requirement, shown in Fig. 14(a). To determine the set of stable manifold trajectories whose perigee is lower than the distance threshold for aerobraking ($r_{threshold}$ = 6478 km), the relationship between the distance of the perigee of the stable manifold and

the parameter t_p is obtained, shown in Fig. 14(b). Therefore, we define the set of t_p which determines the perigee distance of the stable manifold to the centre of the Earth in the interval [r_{Earth}, $r_{threshold}$] as the aerobraking window. As shown in Fig. 14(b), for a Lyapunov orbit with J = 3.00079830, the aerobraking window is $\{t_p \,|\, t_p \in (1.6163, 1.6188] \cup t_p \in (2.0227, 2.0253]\}$.

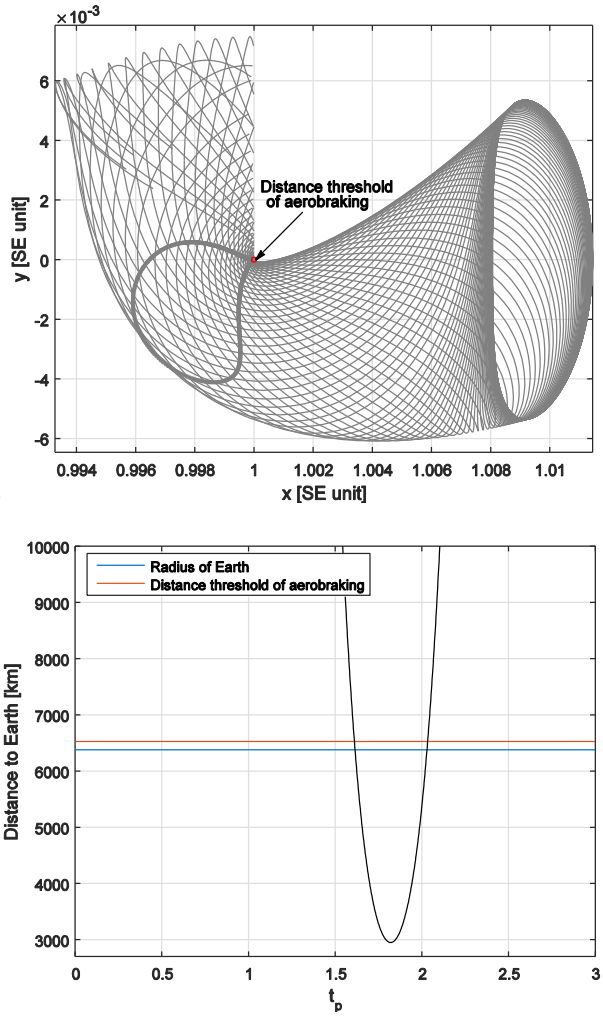

Figure 14. Given a Sun-Earth L_2 Lyapunov orbit with J = 3.00079830, (a) the periapis map of the stable manifolds and (b) the relationship between the distance of the perigee of the stable manifolds and the parameter t_p.

6.4 Design Procedure and Optimization

The process of designing the transfer trajectory for NEA capture using aerobraking is similar to Section 5.3 and is as follows:

(1) Select one target NEA in the candidate catalogue (e.g. 2009UJ) in Fig. 5;

(2) Given the Jacobi constant J and t_p at the aerobraking window, which is obtained in Section 6.2, the stable manifold associated with the periodic orbit is propagated backward until it reaches the perigee and then the state $\boldsymbol{S}_{p+} = [x_p, y_p, z_p, \dot{x}_{p+}, \dot{y}_{p+}, \dot{z}_{p+}]^T$ at perigee in the Sun-Earth rotating frame is obtained, shown in Fig. 15;

(3) The velocity $\boldsymbol{V}_{p-}$ before aerobraking in the Earth-centred inertial frame can then be calculated and the state of the NEA $\boldsymbol{S}_{p-} = [x_p, y_p, z_p, \dot{x}_{p-}, \dot{y}_{p-}, \dot{z}_{p-}]^T$ before aerobraking in the Sun-Earth rotating frame can be obtained using Eq. (25);

(4) Given the flight time T_{fly2}, the state $\boldsymbol{S}_{p-}$ is propagated backward and then the target point $\boldsymbol{S}_f$ is obtained, shown in Fig. 16;

(5) Given a departure date T_0, transform the initial state of the candidate NEA in the Sun-centred inertial frame to the Sun-Earth rotating frame so that $\boldsymbol{S}_i$ is then obtained;

(6) Given the flight time T_{fly1}, Eq. (14) is then applied to design the transfer between the candidate NEA's initial orbit $\boldsymbol{S}_i$ and the target points $\boldsymbol{S}_f$. Thus, the manoeuvres Δv_1 and Δv_2 can be calculated.

Then, the total cost of capturing the NEA onto the target Sun-Earth L_1 or L_2 periodic orbit with aerobraking can be obtained by using Eq. (15). The transfer trajectory is shown in Fig. 17 and Fig. 18. The 5 parameters (T_0, T_{fly1}, T_{fly2}, J, t_p) associated with the transfers from the candidate NEA initial orbit to the stable manifold can be optimised using NSGA-II, again using the total cost Δv as the objective function. The optimal results of capturing NEAs onto the Sun-Earth L_1 and L_2 Lyapunov orbits are shown in Table 3.

Comparing the results of Table 2 and Table 3, we find that aerobraking can save energy and so the capture strategy has the potential to be cheaper than the NEA capture strategy without a flyby. Moreover, the NEA capture strategy using aerobraking also has the potential to require a shorter flight time, as does the capture strategy using the Earth flyby without aerobraking. Moreover, comparing the results in Table 1 and Table 3, we find that aerobraking can provide a manoeuvre which can help to achieve cheaper NEA capture than the strategy using the Earth flyby without aerobraking, e.g. 2006UQ216, 2011BQ50 and 2010UJ, et al. However, for the practical implementation of the NEA capture strategy using aerobraking, it is necessary to take into account the real ephemeris model and a more accurate atmosphere model. The preliminary results in this paper can serve as approximations for such real missions. Considering the sensitivity of the transfer trajectory in the Sun-Earth CRTBP, especially the aerobraking phase, an accurate navigation and control strategy would be required to guarantee that the fly-by of the candidate NEA is at required altitude in order to obtain the required aerobraking manoeuvre. For example, the drag-modulation flight control method (Putnam and Braun, 2013) and the blended control,

predictor-corrector guidance algorithm (Jits and Walberg, 2004) may provide feasible solutions for the asteroid capture mission using aerobraking. Again, the carrier spacecraft is envisaged as remaining attached to, and shielded, by the NEA during the aerobraking manoeuvre to deliver active control.

Assuming that a high thrust engine of specific impulse (I_{sp}) 300 s is utilized to capture candidate asteroids, the required propellant mass of the spacecraft is appended for each trajectory in Tables 1-3. Here we assume that a spacecraft of 5500 kg dry mass and 8100 kg of propellant is already at the NEA encounter, an example from the Keck study report for asteroid retrieval (Brophy et al., 2012). Then we set 8100 kg as the threshold of the required propellant mass to investigate the possibility of capturing asteroids with current technology. From Table 3, we find that 2014AA, 2014WE6, 2014WX202 can be captured onto Sun-Earth L_1/L_2 Lyapunov orbits with a propellant mass of less than 8100 kg. On the other hand, if a low-thrust engine of higher specific impulse (e.g., 3000 s) can be utilized to capture these asteroids, the required propellant mass would be approximately one-tenth that of the high-thrust case, and thus many more asteroids could be captured, e.g. 2007UN12, 2008UA202 and 2012WR10. Furthermore, for those asteroids which cannot be captured even with a low-thrust engine of much higher specific impulse, the possibility of capturing a segment from such asteroids would be also of scientific and technological interest.

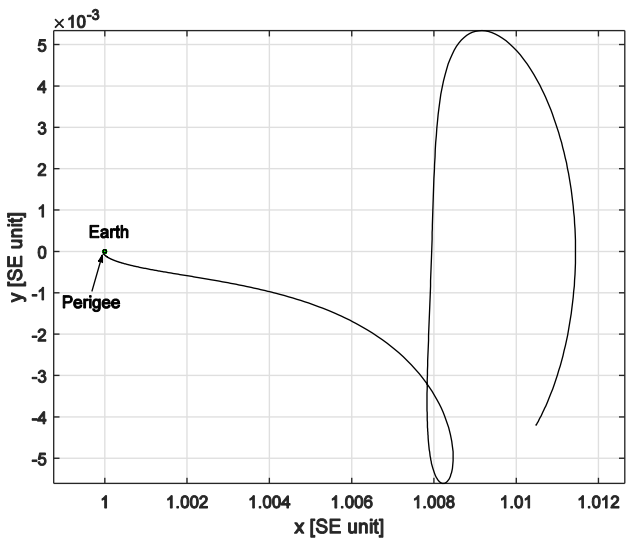

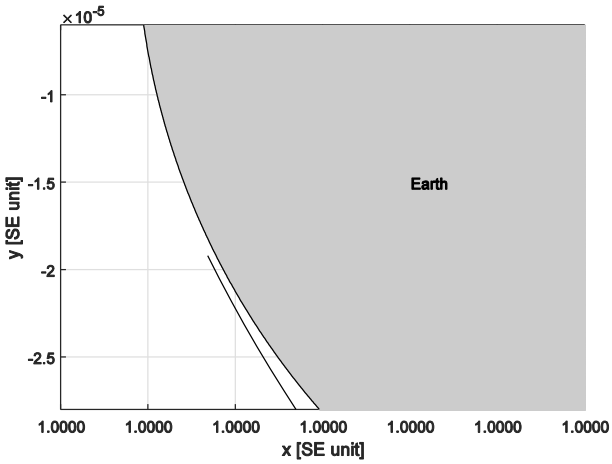

Figure 15. Given C =3.00079830, t_p=1.617219, the stable manifold associated with the Sun-Earth L_2 Lyapunov orbit and its perigee.

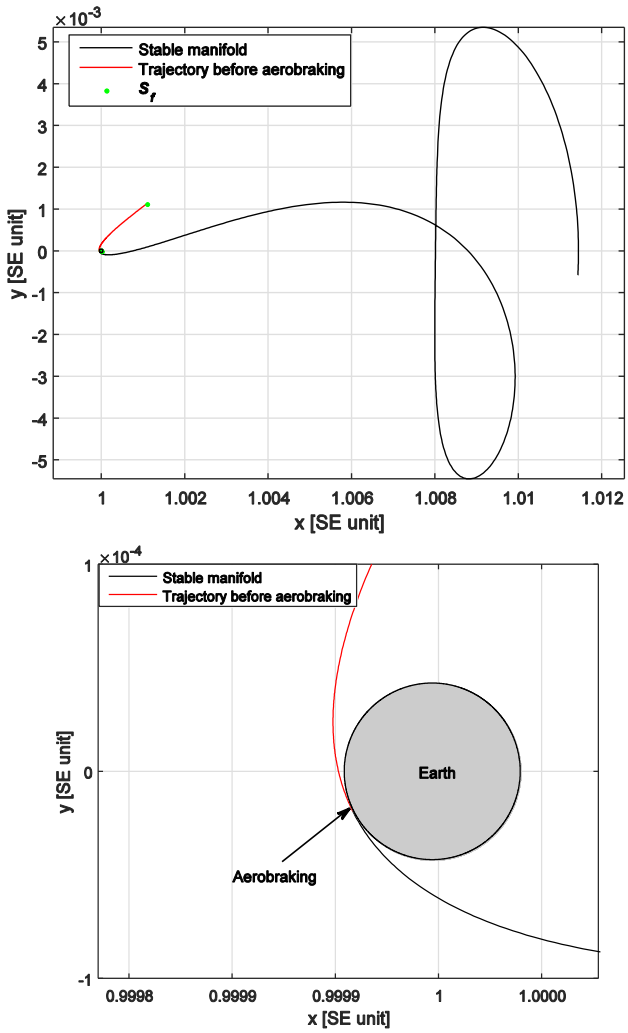

Figure 16. Given T_{fly2} = 0.465127, the trajectory before aerobraking is obtained by propagating backward from the state at perigee.

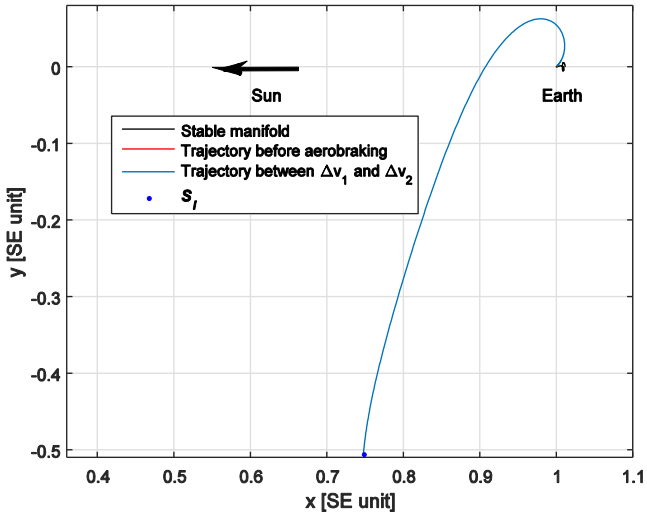

Figure 17. Given T_0 = 59284.5 [MJD], T_{fly1} = 4.295717, the transfer trajectory (*xy* projection) for capturing 2010UJ onto the Sun-Earth L_2 Lyapunov orbit in the Sun-Earth rotating frame.

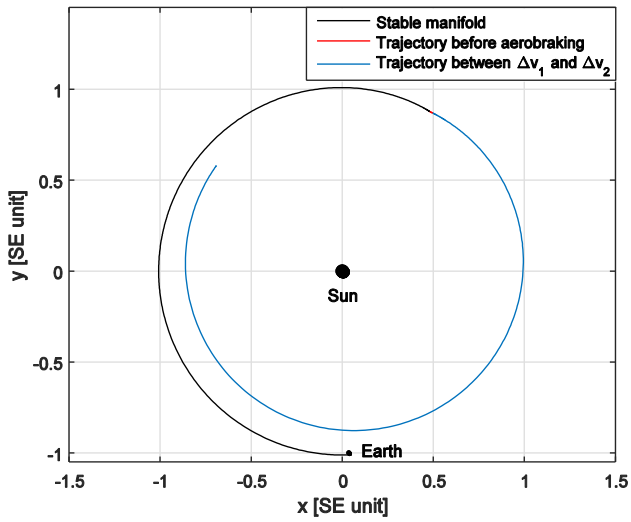

Figure 18. Transfer trajectory (*xy* projection) for capturing 2010UJ onto the Sun-Earth L_2 Lyapunov orbit in the Sun-centred inertial frame.

Table 3 Results of capturing NEAs onto Sun-Earth L_2 Lyapunov orbits using aerobraking

NEA	Total cost, m/s	Epoch, MJD	Total flight time, days	Jacobi constant of Lyapunov orbit	Propellant mass, ton	Target point
2003WT153	445.60	58469.4	516.5	3.00009708	115.7	L_1
2006UQ216	388.60	61719.4	1004.5	3.00009708	267.8	L_1
2007UN12	152.72	58624.8	745.3	3.00022611	15.8	L_1
2008EL68	626.26	58800.1	1156.1	3.00022894	239	L_1
2008JL24	728.08	59427.7	1254.5	3.00022966	19.8	L_1

2008UA202	241.56	61145.5	1316.5	3.00076914	9.4	L_2
2009YR	536.24	58214.4	825.0	3.00066561	137.2	L_2
2010JR34	526.59	60194.6	1119.0	3.00074606	204.2	L_2
2010UJ	323.31	59284.5	469.9	3.00079830	1029.4	L_2
2010UY7	596.27	58853.8	905.4	3.00022482	75.7	L_1
2010VQ	321.37	58275.4	386.7	3.00079251	128.9	L_2
2011BQ50	512.82	59625.5	535.1	3.00077442	131.7	L_1
2011BQ50	311.07	59478.4	1098.6	3.00079413	82.5	L_2
2011CL50	134.67	58395.3	1063.5	3.00063389	63.9	L_1
2012HG2	434.51	60247.1	849.3	3.00079477	449.9	L_2
2012WR10	243.16	61179.0	1517.1	3.00022471	24.8	L_1
2014AA	1091.77	58207.2	847.3	3.00080146	4.6	L_2
2014JR24	628.59	60200.0	1152.4	3.00009610	26.3	L_1
2014UV210	350.07	58452.2	605.3	3.00022906	421.9	L_1
2014UV210	393.26	58629.2	598.4	3.00059545	470.6	L_2
2014WE6	715.03	63975.2	1002.7	3.0007983	6.4	L_2
2014WX202	278.53	63098.7	1379.4	3.00063389	8.1	L_1
2015PS228	613.58	63417.0	735.5	3.00009617	42.3	L_1

6.5 Extension to the full Ephemeris Model

In a real mission of capturing asteroids around the Sun-Earth libration points, the perturbations, including the eccentricity and inclination of the Earth's orbit around the Sun, the Moon's gravity should be considered. Here a Sun-centered J2000 inertial frame is utilized to describe the motion of captured asteroids in the full ephemeris dynamical model. The position and velocity vector of each body are obtained from the DE421 ephemerides (Folkner et al., 2008). Therefore, the equation of motion of the captured asteroid in the Sun-centered inertial frame can be written as

$$\ddot{\boldsymbol{r}} = -\frac{\mu_{Sun}}{r^3}\boldsymbol{r} - \sum_{i=1}^{9}\frac{\mu_i}{\|\boldsymbol{r}-\boldsymbol{r}_i\|^3}(\boldsymbol{r}-\boldsymbol{r}_i) \tag{17}$$

where $\boldsymbol{r}$ is the position vector of the asteroid with respect to the Sun; μ_i is the gravitational constants of the planets (Mercury, Venus, Earth, Mars, Jupiter, Saturn, Uranus, Neptune) or the Moon; $\boldsymbol{r}_i$ is the position vector of the planets or the Moon with respect to the Sun.

Since the Sun-Earth CRTBP model assumes that Earth moves on a circular orbit around the Sun without considering any perturbations, the final target orbits are no longer periodic in the full ephemeris dynamical model. A control strategy is therefore required to maintain a captured asteroid in an orbit around a libration point. Thus, here we still assume that the initial state of the stable manifold is generated from the Lyapunov orbit, as shown in Section 2.2 and then the transfer trajectory of capturing an asteroid will be propagated backwards. The first step is to move the state from the Sun-Earth rotating system to the Sun-centered J2000 inertial system. Assuming that the position vector and velocity vector of the stable manifold's initial state in the Sun-Earth rotating frame are $\boldsymbol{R}_m^r$ and $\boldsymbol{V}_m^r$, respectively, the position vector and velocity vector of the stable manifold's initial state in the Sun-centered J2000 inertial frame can be calculated as follows (Kolemen et al., 2012)

$$\boldsymbol{R}_m^i = \boldsymbol{M}_{rot}\boldsymbol{R}_{syn}^r + \boldsymbol{R}_e^i, \boldsymbol{V}_m^i = \boldsymbol{M}_{rot}\boldsymbol{V}_{syn}^r + \boldsymbol{\omega}\times(\boldsymbol{M}_{rot}\boldsymbol{R}_{syn}^r) + \boldsymbol{V}_e^i, \tag{18}$$

where

$$\boldsymbol{\omega} = \frac{\boldsymbol{R}_e^i \times \boldsymbol{V}_e^i}{\left\|\boldsymbol{R}_e^i \times \boldsymbol{V}_e^i\right\|}, \boldsymbol{M}_{rot} = [\boldsymbol{e}_1 \quad \boldsymbol{e}_2 \quad \boldsymbol{e}_3], \boldsymbol{e}_1 = \frac{\boldsymbol{R}_e^i}{\left\|\boldsymbol{R}_e^i\right\|}, \boldsymbol{e}_3 = \frac{\boldsymbol{\omega}}{\left\|\boldsymbol{\omega}\right\|}, \boldsymbol{e}_2 = \frac{\boldsymbol{e}_1 \times \boldsymbol{e}_3}{\left\|\boldsymbol{e}_1 \times \boldsymbol{e}_3\right\|}$$

$$\boldsymbol{R}_{syn}^r = \left\|\boldsymbol{R}_e^i\right\|(\boldsymbol{R}_m^r - [1-\mu \quad 0 \quad 0]^T), \boldsymbol{V}_{syn}^r = \left\|\boldsymbol{R}_e^i\right\|\left\|\boldsymbol{\omega}\right\|\boldsymbol{V}_m^r$$

and $\boldsymbol{R}_e^i$, $\boldsymbol{V}_e^i$ are the position vector and velocity vector of the Earth in the Sun-centered J2000 inertial frame.

Then the stable manifold's initial state in the Sun-centered J2000 inertial frame is propagated backwards until it reaches perigee. At perigee, the state of the captured asteroid before aerobraking can then be calculated, as stated in Section 6.2. Moreover, the state before aerobraking will be propagated backwards in the full ephemeris dynamical model with a given flight time and then the target point obtained. Therefore, the total cost of capturing an asteroid can be calculated by solving the Lambert arc between the asteroid's orbit and the target periodic orbit in the full ephemeris dynamical model. According to the design procedure stated above, an example of capturing 2010UJ onto Sun-Earth L_2 Lyapunov orbits in the full ephemeris dynamical model is investigated and the transfer trajectory for capture is shown in Fig. 19. The total cost of capturing 2010UJ is Δv = 379.42 m/s when the epoch T_0 = 59100.3 MJD, the total flight time T_{fly} = 665.9 days and the Jacobi constant of the Lyapunov orbit is J = 3.00076653. The results of capturing 2010UJ in the full ephemeris dynamical model and in the Sun-Earth CRTBP model are

slightly different. The total cost of capturing this asteroid in the full ephemeris dynamical model is about 17% more than that in the Sun-Earth CRTBP model. However, the Sun-Earth CRTBP is still a good first-order approximation to the real Solar System dynamics (Kolemen et al., 2012). Furthermore, the family of candidate asteroids which can be captured with low cost in the Sun-Earth CRTBP model are not expected to change and thus they can also serve as candidate asteroids which can be captured with low cost in the full ephemeris dynamical model.

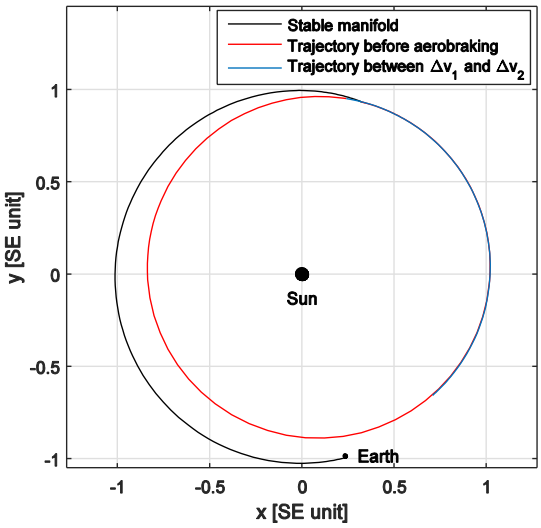

Figure 19. Transfer trajectory (*x*-*y* projection) for capturing 2010UJ in the Sun-centred J2000 inertial frame.

7. Conclusions

The possibility of capturing small NEAs using low energy transfers would in principle be of significant scientific and commercial interest. Although NEAs may make close approaches to the Earth, and so represent a potential impact threat, the exploitation of their resources has long been proposed as a necessary element for future space exploration.

As an ideal location for space science, and a staging node for interplanetary missions in the future, the Sun-Earth L_1/L_2 libration points are likely to play an important role for future space exploration. Therefore, capturing asteroids onto periodic orbits around the Sun-Earth L_1/L_2 points is of particular interest. A strategy to couple a flyby of the Earth to stable manifolds to capture NEAs onto Sun–Earth L_1/L_2 periodic orbits has been proposed. In this capture strategy the candidate NEA is first assumed to leave its orbit with an impulse manoeuvre and will then approach the vicinity of the Earth for the flyby. During the flyby, the Earth's atmosphere may also provide an aerobraking manoeuvre. If not, a propulsive manoeuvre is required at the perigee of the flyby. After the flyby of the Earth,

the candidate NEA inserts onto the stable manifold associated with a periodic orbit around the Sun-Earth L_1 or L_2 points and will be asymptotically captured onto it.

Comparing the results of two methods, it is found that NEA capture strategies using an Earth flyby with and without the aerobraking both have the potential to be cheaper (in terms of Δv) than direct stable manifold capture. Besides, due to the fact that direct capture without a flyby requires significant additional time to move along the stable manifolds of the Sun–Earth L_1/L_2 periodic orbits, NEA capture strategies using Earth flyby also have the potential to save flight time.

Acknowledgments

We acknowledge support through the China Scholarship Council (Minghu Tan) and a Royal Society Wolfson Research Merit Award (Colin McInnes).

References

Bao, C., Yang, H., Barsbold, B., Baoyin, H., 2015. Capturing near-Earth asteroids into bounded Earth orbits using gravity assist. Astrophys. Space Sci. 360, 61. https://doi.org/10.1007/s10509-015-2581-3.

Belbruno, E.A., Miller, J.K., 1993. Sun-perturbed Earth-to-Moon transfers with ballistic capture. J. Guid. Contr. Dynam. 16(4), 770-775. https://doi.org/10.2514/3.21079.

Bottke, W.F., 2002. Asteroids III. University of Arizona Press, Tucson.

Brophy, J.R., Friedman, L., Culick, F., 2012. Asteroid retrieval feasibility. Keck Institute for Space Studies, California Institute of Technology, Jet Propulsion Laboratory, Report 1457705567, Pasadena, California.

Casalino, L., Colasurdo, G., 2003. Mars gravity assist to improve missions towards main-belt asteroids. Acta Astronaut. 53(4-10), 521-526. https://doi.org/10.1016/S0094-5765(03)80012-7.

Ceriotti, M., 2010. Global optimisation of multiple gravity assist trajectories. University of Glasgow.

Chen, Y., Baoyin, H., Li, J., 2014. Accessibility of main-belt asteroids via gravity assists. J. Guid. Contr. Dynam. 37(2), 623-632. https://doi.org/10.2514/1.58935.

Chesley, S.R., Chodas, P.W., Milani, A., Valsecchi, G.B., Yeomans, D.K., 2002. Quantifying the risk posed by potential Earth impacts. Icarus 159(2), 423-432. https://doi.org/10.1006/icar.2002.6910.

Davis, K.E., Anderson, R.L., Scheeres, D.J., Born, G.H., 2010. The use of invariant manifolds for transfers between unstable periodic orbits of different energies. Celest. Mech. Dyn. Astron 107(4), 471-485. https://doi.org/10.1007/s10569-010-9285-3.

Davis, K.E., Anderson, R.L., Scheeres, D.J., Born, G.H., 2011. Optimal transfers between unstable periodic orbits using invariant manifolds. Celest. Mech. Dyn. Astron 109(3), 241-264. https://doi.org/10.1007/s10569-010-9327-x.

Deb, K., Pratap, A., Agarwal, S., Meyarivan, T., 2002. A fast and elitist multiobjective genetic algorithm: NSGA-II. IEEE Trans. Evol. 6(2), 182-197. https://doi.org/10.1109/4235.996017.

Eismont, N., Boyarskii, M., Ledkov, A., Nazirov, R., Dunham, D., Shustov, B., 2013. On the possibility of the guidance of small asteroids to dangerous celestial bodies using the gravity-assist maneuver. Sol. Syst. Res. 47(4), 325-333. https://doi.org/10.1134/S0038094613040102.

Farquhar, R.W., Dunham, D.W., Guo, Y., McAdams, J.V., 2004. Utilization of libration points for human exploration in the Sun–Earth–Moon system and beyond. Acta Astronaut. 55(3), 687-700. https://doi.org/10.1016/j.actaastro.2004.05.021.

Folkner, W.M., Williams, J.G., Boggs, D.H., 2008. The planetary and lunar ephemeris DE 421. JPL IOM 343R-08-003.

Folta, D.C., Woodard, M., Howell, K., Patterson, C., Schlei, W., 2012. Applications of multi-body dynamical environments: the ARTEMIS transfer trajectory design. Acta Astronaut. 73, 237-249. https://doi.org/10.1016/j.actaastro.2011.11.007.

Gómez, G., 2001. Dynamics and Mission Design Near Libration Points, Vol I: Fundamentals: the Case of Collinear Libration Points. World Scientific, Singapore.

Gao, Y., 2013. Near-Earth asteroid flyby trajectories from the Sun-Earth L2 for Chang'e-2's extended flight. Acta Mechanica Sinica 29(1), 123-131. https://doi.org/10.1007/s10409-013-0011-8.

Gong, S., Li, J., 2015. Asteroid capture using lunar flyby. Adv. Space Res. 56(5), 848-858. https://doi.org/10.1016/j.asr.2015.05.020.

Grebow, D.J., 2010. Trajectory design in the Earth-Moon system and lunar South Pole coverage. Purdue University.

Hasnain, Z., Lamb, C.A., Ross, S.D., 2012. Capturing near-Earth asteroids around Earth. Acta Astronaut. 81(2), 523-531. https://doi.org/10.1016/j.actaastro.2012.07.029.

Henon, M., 2003. New families of periodic orbits in Hill's problem of three bodies. Celest. Mech. Dyn. Astron 85(3), 223-246. https://doi.org/10.1023/A:1022518422926.

Heppenheimer, T., 1971. Approximate analytic modeling of a ballistic aerobraking planetary capture. J. Spacecrat Rockets 8(5), 554-555. https://doi.org/10.2514/3.30311.

Howell, K.C., Davis, D.C., Haapala, A.F., 2011. Application of periapse maps for the design of trajectories near the smaller primary in multi-body regimes. Math. Probl. Eng. 2012, 1-22. https://doi.org/10.1155/2012/351759.

Howell, K.C., Kakoi, M., 2006. Transfers between the Earth–Moon and Sun–Earth systems using manifolds and transit orbits. Acta Astronaut. 59(1), 367-380. https://doi.org/10.1016/j.actaastro.2006.02.010.

Jits, R.Y., Walberg, G.D., 2004. Blended control, predictor–corrector guidance algorithm: an enabling technology for Mars aerocapture. Acta Astronaut. 54(6), 385-398. https://doi.org/10.1016/S0094-5765(03)00159-0.

Keller, H.B., 1976. Numerical solution of two point boundary value problems. SIAM Regional Conference Series in Applied Mathematics, J. W. Arrowsmith Ltd., Bristol, England, U.K.

Kolemen, E., Kasdin, N.J., Gurfil, P., 2012. Multiple Poincaré sections method for finding the quasiperiodic orbits of the restricted three body problem. Celest. Mech. Dyn. Astron 112(1), 47-74. https://doi.org/10.1007/s10569-011-9383-x.

Koon, W., Lo, M., Marsden, J., Ross, S., 2001. Low Energy Transfer to the Moon. Celest. Mech. Dyn. Astron 81(1-2), 63-73. https://doi.org/10.1023/A:1013359120468.

Koon, W.S., Lo, M.W., Marsden, J.E., Ross, S.D., 2000. Shoot the moon. Proceedings of Spaceflight Mechanics 2000. San Diego, CA, pp. 1017-1030.

Koon, W.S., Lo, M.W., Marsden, J.E., Ross, S.D., 2011. Dynamical systems, the three-body problem and space mission design. Springer-Verlag, New York.

Lei, H., Xu, B., 2016. Transfers between libration point orbits of Sun–Earth and Earth–Moon systems by using invariant manifolds. J. Eng. Math. 98(1), 163-186. https://doi.org/10.1007/s10665-015-9816-8.

Lewis, J.S., Hutson, M.L., 1993. Resources of near-Earth space. University of Arizona Press, Tucson Arizona.

Lladó, N., Ren, Y., Masdemont, J.J., Gómez, G., 2014. Capturing small asteroids into a Sun–Earth Lagrangian point. Acta Astronaut. 95, 176-188. https://doi.org/10.1016/j.actaastro.2013.11.007.

Lo, M.W., Parker, J.S., 2004. Unstable resonant orbits near earth and their applications in planetary missions. AIAA/AAS Astrodynamics Specialist Conference. Providence, RI. Paper AIAA 2004-5304.

Mingotti, G., Sánchez, J., McInnes, C., 2014. Combined low-thrust propulsion and invariant manifold trajectories to capture NEOs in the Sun–Earth circular restricted three-body problem. Celest. Mech. Dyn. Astron 120(3), 309-336. https://doi.org/10.1007/s10569-014-9589-9.

Minovitch, M.A., 2010. The invention that opened the solar system to exploration. Planet. Space Sci. 58(6), 885-892. https://doi.org/10.1016/j.pss.2010.01.008.

Pavlak, T.A., 2013. Trajectory design and orbit maintenance strategies in multi-body dynamical regimes. Purdue University.

Putnam, Z.R., Braun, R.D., 2013. Drag-modulation flight-control system options for planetary aerocapture. J. Spacecrat Rockets 51(1), 139-150. https://doi.org/10.2514/1.A32589.

Qiao, D., Cui, H., Cui, P., 2006. Evaluating accessibility of near-earth asteroids via earth gravity assists. J. Guid. Contr. Dynam. 29(2), 502-505. https://doi.org/10.2514/1.16757.

Richardson, D.L., 1980. Analytic construction of periodic orbits about the collinear points. Celest. Mech. 22(3), 241-253. https://doi.org/10.1007/BF01229511.

Sánchez, J.P., Yárnoz, D.G., 2016. Asteroid retrieval missions enabled by invariant manifold dynamics. Acta Astronaut. 127, 667-677. https://doi.org/10.1016/j.actaastro.2016.05.034.

Sanchez, J.P., Garcia Yarnoz, D., Alessi, E.M., McInnes, C., 2012. Gravitational capture opportunites for asteroid retrieval missions. 63rd International Astronautical Congress. Naples, Italy. Paper IAC-12.C1.5.13x14763.

Sanchez, J.P., Garcia Yarnoz, D., McInnes, C., 2012. Near-Earth asteroid resource accessibility and future capture mission opportunities. Global Space Exploration Conference. Washington, DC. Paper GLEX-2012.11.1.5x12412.

Sanchez, J.P., McInnes, C., 2012. Synergistic approach of asteroid exploitation and planetary protection. Adv. Space Res. 49(4), 667-685. https://doi.org/10.1016/j.asr.2011.11.014.

Sonter, M.J., 1997. The technical and economic feasibility of mining the near-earth asteroids. Acta Astronaut. 41(4-10), 637-647. https://doi.org/10.1016/S0094-5765(98)00087-3.

Szebehely, V., 1967. Theory of orbit: The restricted problem of three Bodies. Academic Press, New York.

Tang, G., Jiang, F., 2016. Capture of near-Earth objects with low-thrust propulsion and invariant manifolds. Astrophys. Space Sci. 361(1), 1-14. https://doi.org/10.1007/s10509-015-2592-0.

Vallado, D.A., 2007. Fundamentals of astrodynamics and applications. Springer, New York.

Vasile, M., Colombo, C., 2008. Optimal impact strategies for asteroid deflection. J. Guid. Contr. Dynam. 31(4), 858-872. https://doi.org/10.2514/1.33432.

Vasile, M., Pascale, P.D., 2006. Preliminary design of multiple gravity-assist trajectories. J. Spacecrat Rockets 43(4), 794-805. https://doi.org/10.2514/1.17413.

Villac, B., Scheeres, D.J., 2003. Escaping trajectories in the Hill three-body problem and applications. J. Guid. Contr. Dynam. 26(2), 224-232. https://doi.org/10.2514/2.5062.

Wang, Y.M., Qiao, D., Cui, P.Y., 2013. Trajectory Design for the Transfer from the Lissajous Orbit of Sun-Earth System to Asteroids. Appl. Mech. Mater. 390, 478-484. https://doi.org/10.4028/www.scientific.net/AMM.390.478.

Xu, M., Tan, T., Xu, S., 2012. Research on the transfers to Halo orbits from the view of invariant manifolds. Sci. China Phys. Mech. 55(4), 671-683. https://doi.org/10.1007/s11433-012-4680-2.

Yárnoz, D.G., Sanchez, J.-P., McInnes, C.R., 2013. Opportunities for asteroid retrieval missions. *Asteroids.* Berlin: Springer, pp. 479-505.

Yárnoz, D.G., Sanchez, J., McInnes, C., 2013. Easily retrievable objects among the NEO population. Celest. Mech. Dyn. Astron 116(4), 367-388. https://doi.org/10.1007/s10569-013-9495-6.

Yang, H., Li, J., Baoyin, H., 2015. Low-cost transfer between asteroids with distant orbits using multiple gravity assists. Adv. Space Res. 56(5), 837-847. https://doi.org/10.1016/j.asr.2015.05.013.

Zimmer, A., 2013. Investigation of vehicle reusability for human exploration of Near-Earth Asteroids using Sun–Earth Libration point orbits. Acta Astronaut. 90(1), 119-128. https://doi.org/10.1016/j.actaastro.2012.10.003.